CRYSTAL GROWTH & DESIGN

pubs.acs.org/crystal

Review

X-ray Diffraction Topography (Imaging) of Crystals Grown from Solution: A Short Review

Published as part of a Crystal Growth and Design virtual special issue Celebrating John N. Sherwood, Pioneer in Organic and Molecular Crystals

Brian K. Tanner*

Cite This: *Cryst. Growth Des.* 2023, 23, 3026−3033

Read Online

ACCESS | Metrics & More | Article Recommendations

ABSTRACT: A short review of X-ray topographic studies of crystals grown from solution is presented. The dislocation configurations characteristic of such crystals are described, and Klapper's explanation in terms of minimization of the elastic energy of a dislocation per unit growth length is highlighted. It is shown that the principles apply to crystals grown not only from low temperature solution but also by hydrothermal growth and growth from fluxed melts. Recent studies of growth of protein crystals have found that they have similar dislocation configurations and characteristics to those of ionic and small organic molecule crystals grown from solution.

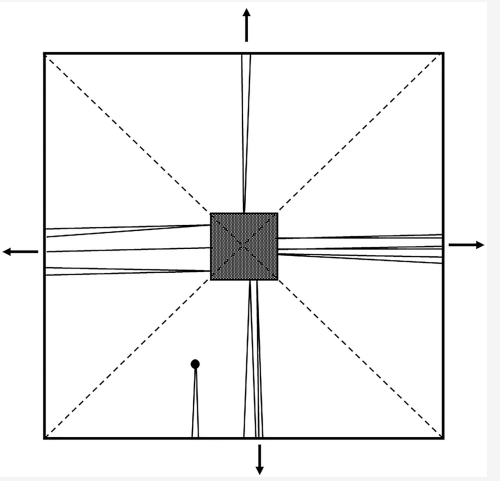

INTRODUCTION

X-ray topography or X-ray diffraction imaging has its origins nearly a century ago when, in 1931, Wolfgang Berg noted that the scattering power across a rock salt crystal illuminated by a divergent X-ray beam was not uniform. Contrast corresponding to the traces of slip planes was observed following compression and subsequent annealing.[1] From these beginnings, the techniques have developed to a point where cracks propagating at up to 2.5 km s^{-1} can now be imaged directly on the microsecond time scale.[2]

While Berg's and subsequently Barrett's 1945 methods exploited the characteristic lines,[3] in 1954 Schulz used the continuous part of the X-ray spectrum, observing diffraction contrast across crystals in the Laue technique.[4] It was this white beam method that Turkka Tuomi and colleagues used to take transmission X-ray topographs with exposure times of the order of seconds using the newly available sources of synchrotron radiation[5] in 1974. This was quickly exploited to perform quasi-static studies of transient phenomena in nonambient environments.[6,7]

Most of the applications of X-ray topography have been in the study of dislocations, both generated by slip and through the relaxation of strains in growing crystals. Such latter dislocations form particularly striking configurations in crystals grown from solution, and it was in their study, by X-ray topography both in the laboratory and at synchrotron radiation sources, that John Sherwood made a significant contribution.

X-RAY TOPOGRAPHY TECHNIQUES

Full details of X-ray topography methods and analysis can be found in books by the present author,[8−10] and there are more recent short reviews of techniques[11] and applications.[12] Therefore, only those techniques most frequently associated with analysis of crystals grown from solution will be described in this section, these also being those which John Sherwood and colleagues used regularly.

Lang's Section and Projection Methods. Extensive use of X-ray topography began following Lang's 1958 observation of individual dislocations[13] in X-ray images using what he called

Published: March 10, 2023

https://doi.org/10.1021/acs.cgd.2c01463
Cryst. Growth Des. 2023, 23, 3026−3033

the Section Topography method. From a small, roughly equiaxed X-ray source, a ribbon beam illuminates the single crystal set to diffract the Kα_1 characteristic line in transmission (Figure 1). Key to the method is that the slit width is small

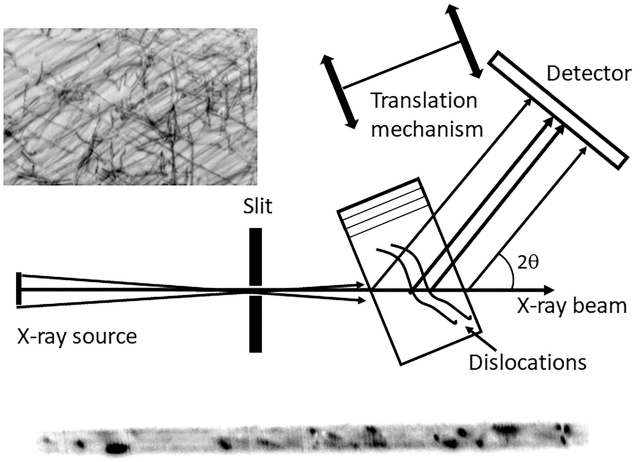

Figure 1. Lang's section and projection (with translation mechanism) techniques of X-ray topography. The bottom image is a section topograph of dislocations in SiC. (Image length 2.3 mm and diffraction vector vertically up the page.) Each black dot corresponds to the intersection of a dislocation with the narrow incident beam. The upper inset shows a projection topograph of the configuration of the dislocations in the same SiC crystal. This shows the distribution of dislocations over the superficial area of the sample. (Field width 1.8 mm.)

compared with the width of the so-called Bormann fan of X-rays diffracted at the entrance and exit surfaces of the crystal. For a typical crystal thickness permitting significant transmission of Kα X-rays from a Mo or Ag target, the slit will be about 10 μm in width. While the geometry permits the energy flow within the crystal to be determined and a detailed analysis of the strains associated with defects to be undertaken, in the context of growth of low atomic number organic crystals it is the ability to image the scattering from a section through a thick crystal that is key. Under low absorption conditions, X-rays are scattered kinematically from the deformed region around a dislocation, enhancing the scattering locally.[8,9] As it is only the narrow ribbon beam that illuminates the dislocation there is a one-to-one correspondence between the enhanced intensity from the dislocation and position where it intersects the ribbon beam. There is therefore no need to cut and polish a low-absorbing crystal in order to determine its internal perfection. A very good example of use of such sectioning to reveal internal defects to be found in one of John Sherwood's last papers, on growth by physical vapor transport of crystals of the nonlinear optical material methyl *p*-hydroxybenzoate.[14]

To view the defects in a large area of a thin crystal, Lang devised a translation mechanism to scan the specimen and detector[15] across the ribbon beam (Figure 1), and it is this Projection Topography method, so-called because it provides a two-dimensional image of the three-dimensional defect structure of the crystal, that is associated with his name. It is the topography technique most widely used in the laboratory.

X-ray Topography at Synchrotron Radiation Sources. At synchrotron radiation sources, topographs can be taken either with the white beam or with a monochromatic beam from a Bragg reflection crystal monochromator, usually a pair of silicon crystals. Because of the huge enhancement of X-ray flux compared with laboratory sources, exposure times are very short and many facilities have high resolution electronic imaging detectors that display images in real time. Experimentally, white beam topography is extremely simple in that the crystal produces a Laue pattern of pseudoimages, each being a topograph. Low precision orientation of the crystal with respect to the incident beam is all that is required to select a reflection of specific wavelength and direction (Figure 2a). With a monochromatic

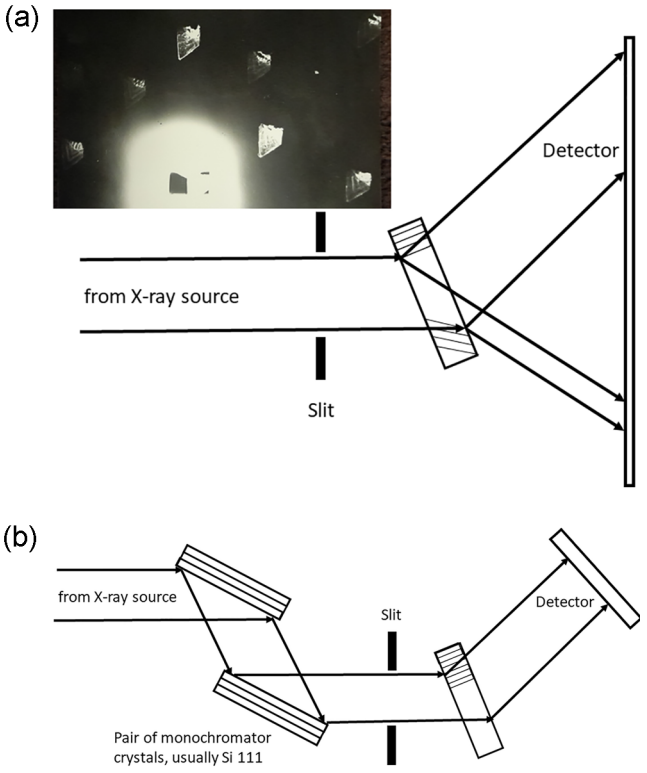

Figure 2. (a) White beam topography using synchrotron radiation. The source is a long way from the experiment, and as the beam is a polychromatic plane wave, a series of Laue spots is obtained from the crystal. Defects result in a different scattering power locally. Inset shows part of a Laue pattern from a thin {111} oriented plate of natural fluorite (see Figure 4). Contrast is seen across individual images. (b) Monochromatic imaging using a pair of crystals to condition the X-ray beam. Diffraction occurs only over a very small range of angles. Lattice distortion around defects results in major change of intensity.

beam, much more precise orientation with respect to the incident beam is required but with modern instrumentation and detectors this is straightforward (Figure 2b). The disadvantage of the white beam technique is that the crystal is exposed to the whole spectrum of radiation. Associated heating through absorption and radiation damage can be a problem for low melting point materials, sometimes limiting beam size and exposure time. Its advantage is that, as the crystal selects its own wavelength for diffraction from the parallel polychromatic beam, bent crystals can yield good quality topographs. This contrasts with the monochromatic mode, where the image is much more sensitive to tilts and dilations, often only resulting in a stripe of intensity across the diffracted beam. However, because of the short exposure times and electronic image processing, it is possible to record multiple images with the crystal at slightly

https://doi.org/10.1021/acs.cgd.2c01463
Cryst. Growth Des. 2023, 23, 3026−3033

different angles with respect to the incident beam and reconstruct an image from the full crystal area in this way.

DISLOCATIONS IN CRYSTALS GROWN FROM SOLUTION

Low Temperature Solution Growth. Prior to the late 1960s, it was assumed that solution-grown crystals, and particularly those of organic materials, contained mosaic structure. However, X-ray topography experiments on NaCl by Ikeno, Maruyama, and Kato,[16] on potash alum by Emara, Lawn, and Lang[17] and on hexamethylene tetramine by Duckett and Lang,[18] revealed that these crystals could be highly perfect, containing very few dislocations. Those that were observed were predominantly long and straight. The early work has been reviewed by Authier.[19]

Klapper[20] distinguished two types of dislocation in solution-grown crystals, those generated during growth and those generated after growth. He presented an example of the latter in slip dislocations in the form of half-loops originating at a small gas bubble in benzil. A more recent example[21] is of closed dislocation loops nucleated at liquid inclusions of *trans*-stilbene ($C_{14}H_{12}$). Of dislocations generated during growth, Klapper further distinguished those that are connected with the growth front and those generated behind the growth front.[22] Dislocations may originate at regions of unstable growth or inclusions of impurity, mother liquor, or gas bubbles. Inclusions and regions of strain frequently occur at the seed surface, and as a result most dislocations in solution grown crystals originate at the seed. If stable growth is then established, in many cases, no further dislocations are nucleated. The dislocation density then decreases as the growing crystal volume increases and the initial dislocations propagate out of the crystal (Figure 3a). Further, as

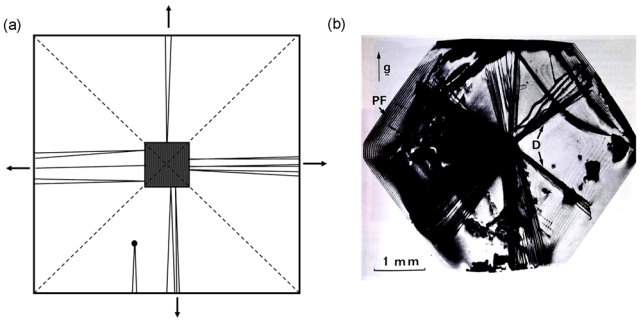

Figure 3. (a) Schematic diagram of an idealized dislocation structure in a relatively elastically isotropic cubic crystal grown from solution on {001} faces. The seed region is the black central section, and the dashed lines represent the boundaries between the growth sectors. The black circle represents an inclusion that has generated a pair of dislocations. (b) Lang topograph of a crystal of solution-grown hexamethylene tetramine. The dislocations D are excellent examples of dislocations running perpendicular to the growth front and the fringes PF are an indication of the perfection of the crystal. Reproduced with permission from Duckett and Lang, ref 18. Copyright Elsevier 1973.

illustrated in references,[8,18,20] because the dislocations originating at the seed grow in specific directions, substantial regions of the crystal can be totally free of dislocations (Figure 3b). Good examples of the various types of growth dislocation in sodium chlorate can be found in the article by Hooper, Roberts, and Sherwood.[23]

In the case of cubic crystals such as NaCl and $NaClO_3$, it was noted that the dislocations generated at the seed ran almost perpendicular to the {100} growth fronts, very different to the configurations previously observed in melt-grown crystals. However, it was found that in crystals exhibiting high elastic anisotropy, some dislocation lines ran in straight lines at distinct and very specific angles to the growth front normal.

An explanation was given and tested by Klapper,[24,25] in terms of minimization of the free energy, associated with the self-energy of the dislocation line, per unit of crystal growth length. A mechanism for achieving this is provided by there being zero force on the dislocation at the position of minimum energy.[26] The elastic self-energy per unit length of a dislocation $E(\boldsymbol{b},\boldsymbol{l},c_{ij})$ may be written as

$$E(\boldsymbol{b}, \boldsymbol{l}, c_{ij}) = K(\boldsymbol{b}, \boldsymbol{l}, c_{ij})(b^2/4\pi) \ln(R/r) \quad (1)$$

where $\boldsymbol{b}$ is the Burgers vector, $\boldsymbol{l}$ is a unit vector in the direction of the dislocation line, and c_{ij} are the elastic constants. The elastic energy per unit length normal to the growth face of the crystal $W(\boldsymbol{b},\boldsymbol{l},\boldsymbol{n},c_{ij})$ is then

$$W(\boldsymbol{b}, \boldsymbol{l}, \boldsymbol{n}, c_{ij}) = E(\boldsymbol{b}, \boldsymbol{l}, c_{ij})/\cos \alpha \quad (2)$$

where $\boldsymbol{n}$ is a unit vector normal to the growth face and $\alpha(\boldsymbol{n},\boldsymbol{l})$ is the angle between the dislocation line direction and the normal to the growth face. As the variation in the logarithmic term of eq 1 is always small, the optimum direction for the dislocation line is determined by the minimization of $K(\boldsymbol{b},\boldsymbol{l},c_{ij})/\cos \alpha$.

Three generic rules emerge from this analysis, which are applicable even if the elastic constants are not known.

1. For a pure screw dislocation $\boldsymbol{l}$ is parallel to $\boldsymbol{n}$.
2. For a pure edge dislocation, provided that $\boldsymbol{n}$ is parallel to a 2-fold symmetry axis, $\boldsymbol{l}$ is parallel to $\boldsymbol{n}$.
3. For a mixed dislocation, $\boldsymbol{l}$ lies between $\boldsymbol{n}$ and $\boldsymbol{b}$.

The model was tested extensively by Klapper[24,25,27,28] and subsequently by other groups. It is reasonably satisfactory in its agreement with experiment, but because it ignores the Peierls energy, which results in dislocations tending to align in crystallographic directions where this is minimized, the model has major limitations. Nevertheless, it explains a number of curious phenomena, such as the refraction of dislocation line directions on crossing growth sector boundaries. In some cases, this change of direction can be up to 30°, such as in ammonium hydrogen oxalate,[28] paracetamol,[29] and the intersection of dislocations with growth bands associated with macrosteps in potassium dihydrogen phosphate (KDP).[30] Studies where the origin of the dislocation configurations can be understood in terms of Klapper's theory include work by Sherwood and colleagues on pentaerythritol tetranitrate[31] (PETN), 2,4,6-trinitrotoluene,[32] and β-cyclotetramethylene tetranitramine (HMX).[33] While extremely useful in explaining the configurations observed in solution-grown crystals, the theory has been disappointingly little used to engineer growth conditions that optimize growth of crystals with low dislocation densities.

High Temperature Hydrothermal Growth. Dislocation configurations found in crystals grown from solution at low temperature have been found to be very similar to those in crystals grown from solution at high temperature. The most important of these, because of its geological prevalence and its industrial importance, is quartz. The first high-resolution study of hydrothermally grown quartz was undertaken in 1967 by Lang and Muiscov,[34] who observed dislocation configurations similar to those in crystals grown from low temperature solutions. Most of the dislocations were nucleated at the seed−crystal interface, and once growth had stabilized, few dislocations were nucleated,

https://doi.org/10.1021/acs.cgd.2c01463
Cryst. Growth Des. 2023, 23, 3026−3033

resulting in some growth sectors being almost dislocation-free. Although the dislocations ran generally parallel to the normal to the growth front, there was considerable dispersion in the angles and relatively few dislocations had screw components. Dislocations tended to cluster into cell walls that correspond to the cobble texture of hillocks and grooves observed on the Z-cut surfaces of synthetic quartz. Shinohara, Iano, and Suzuki[35] subsequently showed that, because of the rapid growth of X and Y sectors, growth on seed crystals with V-shaped notches on Z faces resulted in lower dislocation density crystals. A feature found by Lang and Muiscov[34] was the presence of a strained skin at the surface of the grown crystal, which was shown by Homma and Iwata[36] to be strain associated with a higher sodium concentration than the surrounding material.

Hydrothermally grown calcite was also found to exhibit similar dislocation structures to crystals grown in low temperature solutions. The principle of minimization of the elastic line energy per unit of growth length was found to explain the direction of the dislocation lines.[37]

Where there is an abrupt change in the concentration of impurity incorporated into the growing crystal, the associated strain results in a band of contrast parallel to the growth face being observed in X-ray topographs. These are common in gem-quality mineral crystals such as fluorite (Figure 4) and, together with the growth sector boundary images, permit the growth history of the crystal to be traced. The strain gradient is normal to the growth interface, and the contrast disappears when the diffraction vector $\boldsymbol{g}$ is contained in the plane of the growth face. As exemplified in Figure 4 and elsewhere, the strain at these growth bands can be sufficient to nucleate dislocations. Lefaucheux, Robert, and Authier[38] performed experiments in which the pressure and temperature were abruptly altered in the autoclave during hydrothermal growth of calcite. The nucleated dislocations ran perpendicular to the growth front. These had predominant screw components, and by monitoring the growth history from the growth bands, it was observed that the growth rate increased by up to a factor of 5 when the predominantly screw dislocations were present. A similar dislocation structure can be observed in the natural fluorite crystal shown in Figure 4, where dislocations were nucleated at growth bands and run predominantly perpendicular to the growth fronts.[39]

Similar studies were subsequently conducted by Sherwood et al.[40] on potassium alum where a perturbation in growth conditions was produced by addition of powdered crystals to the solution. It was found that in both cases inclusions were formed at growth bands that generated dislocations which correlated with growth rate enhancement. Previous studies had indicated that edge dislocations contributed to this enhancement.[41,42] Klapper et al.[43] developed this work by introducing perturbations through abrupt changes in temperature during growth by slowly lowering the temperature of the solution. These periods of redissolution resulted in inclusions forming at the growth front with the subsequent generation of dislocations. There was an enhancement of a factor of 6 in the growth rate of the {100} faces compared with the {111} faces following the introduction of the dislocations, which had only pure edge character. Similar dislocations generated at inclusions in the seed regeneration region of crystals of nickel sulfate hexahydrate (α-$NiSO_4{\cdot}6H_2O$) were observed by Masalov et al.,[44] though these dislocations on the {001} faces were of pure screw character.

Growth from Fluxed Melts. High temperature flux growth is a complex form of solution growth, requiring specific regions

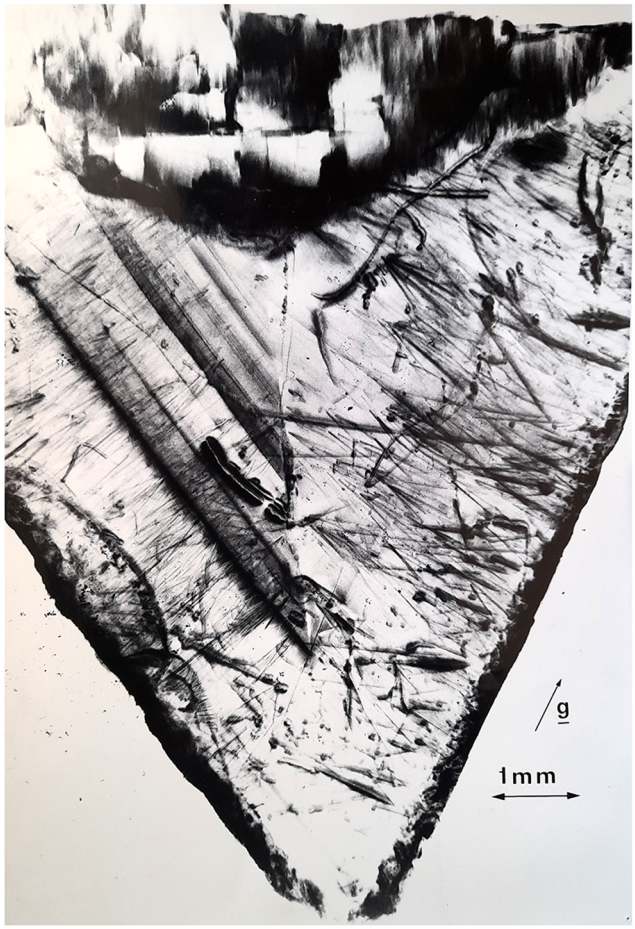

Figure 4. Dislocation and growth band structure of a thin {111} oriented natural fluorite crystal. 220 reflection. Because of the selected diffraction vector, one strong set of growth bands, parallel to the diffraction vector, is invisible in this reflection. Reproduced with permission from ref 39. Copyright The Chemical Society/Royal Society of Chemistry 1977.

of the phase diagram to be accessed. The earliest X-ray topography studies of flux grown crystals were by Austermann and colleagues[45] on beryllium oxide grown from a lithium molybdate flux. They observed screw dislocations in the prism or pyramidal shaped crystal extended in the [0001] direction, the dislocations being presumed to enhance the growth in that direction.

The present author and Oxford colleagues studied a range of flux-grown rare earth vanadate, arsenate, and phosphates and found that the defect configurations had many characteristics of those produced by other methods of solution growth, including the predominance for dislocation lines to run perpendicular to the growth interface. In particular, the strained "skin" found by Lang and Muiscov[34] in hydrothermal quartz was found in RVO_4 (R = Tb, Tm).[46] The directions of growth dislocation lines in the perovskites $KNiF_3$ and $KCoF_3$, grown as cubes with {001} faces by slow cooling from $PbCl_2$-KF-NiF_2 and $PbCl_2$-KF-CoF_2 fluxes, were found to follow well the predictions of the Klapper minimum free energy model.[47] In the example shown in Figure 5, which is a topograph taken with the 002 reflection, there are two types of growth dislocation visible in the (010) growth sector. (Only a few growth bands (E) are visible in this reflection. The very strong growth bands visible in the 020 reflection topographs are invisible in this reflection as the strain

https://doi.org/10.1021/acs.cgd.2c01463
Cryst. Growth Des. 2023, 23, 3026−3033

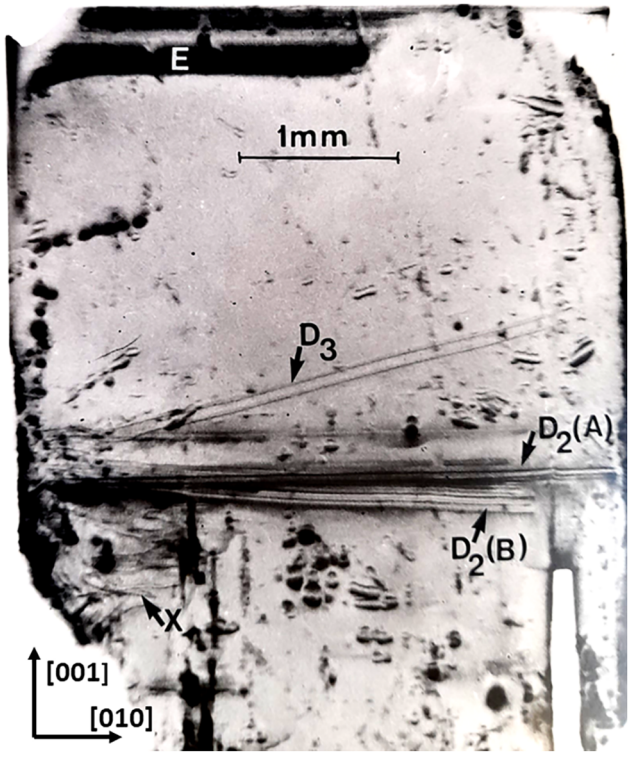

Figure 5. Growth dislocations from a seed point to the left of the image in a flux-grown crystal of $KCoF_3$. Sample surface is in the (100) plane. 002 reflection. Reproduced and adapted with permission from ref 47. Copyright Taylor and Francis 1977.

gradients are normal to the diffraction vector.) The dislocations running parallel to (D_2(A)), or within 5° of (D_2(B)), the [010] normal to the growth front are of pure edge type, while those running at 13 ± 0.5° to [010] (D_3) are of mixed character. Minimization of the elastic line energy per unit growth length yields a prediction of a direction 16° away from [010] for the mixed dislocations.

More recent X-ray topography work on flux-grown crystals has yielded other examples of grown-in dislocation line-directions being in agreement with the theory. Examples include dislocations in $NdAl_3(BO_3)_4$ grown from a BaB_4O_7 flux, which also exhibit the refraction of dislocations on crossing growth sector boundaries.[48] Most growth dislocations observed in flux-grown $RbTiOAsO_4$ ran parallel to the growth surface normal and were of pure edge character.[49] These crystals also contained dislocations generated by inclusions which formed at growth sector boundaries during growth. On the other hand, the majority of dislocations found running normal to the growth face in $KTiOAsO_4$ were predominantly of screw type.[50]

Proteins. It has been known for some time that crystals containing large molecules such as hexamethylbenzene, the units of which are bound by van der Waals forces, could be grown from solution with low defect densities and that the configurations were similar to those of other crystals grown from solution.[51] It has, however, proved harder to demonstrate solution growth of high perfection crystals with larger molecular units, specifically proteins and viruses.[52] Studies using high resolution X-ray diffraction and topography had only modest success.[53−56] Part of the problem was that the very weak scattering of X-rays by the large unit cell protein structures results in a long extinction length ξ_g, which is a measure of the thickness of crystal necessary for dynamical diffraction (or equivalently multiple scattering) effects to be substantial. It was shown some 50 years ago by the present author, using the ubiquitous high perfection material, silicon, that only for crystal thickness greater than about $0.4\xi_g$ would dislocations be visible in Lang topographs.[57] The argument also holds true for white beam synchrotron radiation topographs, and it implies that dislocations will not be visible in small protein crystals using these techniques. Despite the community being aware of this issue, and there being a number of groups trying to visualize dislocations in protein crystals around the turn of the 21st century, it was only with the production of millimeter-size crystals of hen egg white lysozyme (HEWL) that unambiguous images of dislocations in protein crystals were reported.[58,59] Because of the weak scattering, the dislocation images were very wide and of low contrast, but the data were sufficient to establish the Burgers vectors from the $\mathbf{g}\cdot\mathbf{b} = 0$ invisibility criteria. The predominant Burgers vector found in HEWL was ⟨110⟩, of modulus 11.18 nm, resolving the debate as to whether the presence of dislocations with such large Burgers vectors was actually possible in protein crystals.

As crystal quality has improved, it has become possible to use monochromated, beam conditioned, radiation at synchrotron radiation sources to produce narrow, high contrast, images of dislocations in protein crystals. In a parallel, low dispersion, beam of X-rays, strong scattering only occurs within a very small angular range of orientation of the crystal with respect to the incident beam. If the crystal is deliberately offset from this position, strong scattering occurs only when the lattice deformation around the dislocation brings the beam into the correct orientation. This weak beam method, originally developed for transmission electron microscopy, has been increasingly exploited in recent years and provides a mechanism for clarifying dislocation structures in proteins.[60] One of the first applications showed that curved and looped dislocations of Burgers vector were present in HEWL crystals with Burgers vector [010], lying in the $(10\bar{1})$ plane.[61] This is the smallest possible Burgers vector and lowest energy slip plane, presenting evidence of postgrowth plastic deformation through slip in HEWL crystals.

An image of a dislocation configuration in HEWL highly characteristic of solution-grown crystals is to be found in the Supporting Information to the paper of Koizumi et al., a paper primarily concerned with the importance of the hydration state around proteins in growth of high-quality crystals.[62] This beautiful image, reproduced in Figure 6, shows straight dislocations emanating from the seed and running among

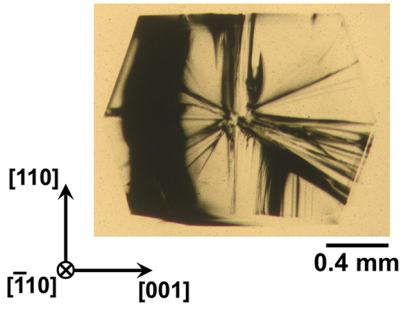

Figure 6. Dislocation configuration in a crystal of hen egg white lysozyme. Reproduced with permission from ref 63. Copyright 2018 American Chemical Society.

https://doi.org/10.1021/acs.cgd.2c01463
Cryst. Growth Des. 2023, 23, 3026−3033

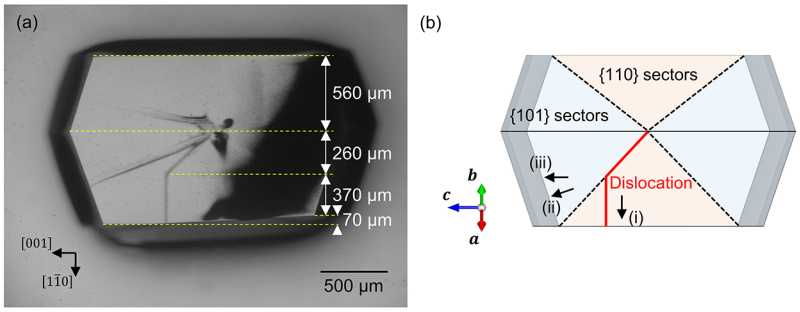

Figure 7. (a) X-ray topograph of hen egg white lysozyme in which a dislocation is refracted on crossing a growth sector boundary. (b) Schematic diagram of the growth sectors and the position of the refraction point. Reproduced from ref 64 with permission of the International Union of Crystallography according to its terms and conditions.

perpendicular to the growth faces.[63] In a more recent paper the same collaboration has produced an example of the refraction of a growth dislocation on crossing a growth sector boundary[64] (Figure 7). The other dislocations visible in this crystal run perpendicular to the growth faces.

The same group has produced many images of similar configurations in HEWL within the Supporting Information to a recent paper in which they used the monochromatic beam imaging capability to identify and measure extremely small twists in crystals of HEWL. These twists are not associated with dislocations and are large in small crystals, the twist period varying as a power law with crystal length.[65] A similar twisting is found in thaumatin, but not glucose isomerase (GI) or ferritin, the latter two having high molecular symmetry.

While most of the studies of dislocations in protein crystals have been done on HEWL, of which large crystals can be grown, this is not the only system to have been studied. Crystals of glucose isomerase have been shown to be even more perfect than HEWL. Dislocation configurations in GI characteristic of solution growth were described by Koizumi et al.[66] and they observed X-ray dynamical diffraction interference fringes from regions of the crystal with varying thickness. Similar dynamical diffraction thickness fringes have been observed in ferritin.[67] In later studies of GI, a crystal was found where only two dislocations propagate from the seed, and these dislocation images exhibit interference fringes corresponding to the difference in distance from the crystal surfaces.[68] These so-called intermediary images are well-known and understood in inorganic materials for whom the product of the linear absorption coefficient and thickness is near unity. Glucose isomerase crystals can be totally free from dislocations, and such crystals have been used to study the effects of radiation damage.[69] Defects, probably dislocations, can be generated at high dose rate, whereas they are not produced at high total dose. Such studies may provide important information on achieving an optimum balance between total dose and dose rate in the minimization of radiation damage during data collection in structural studies.

OUTLOOK

X-ray topography has, without doubt, been a key tool in understanding growth from solution and the defect structures of large crystals. It is vital that expertise in X-ray diffraction imaging is maintained and developed, both at synchrotron radiation facilities and local laboratories, if the defect structure of a wide range of new crystal systems is to be continued to be understood at the macro-scale.

The generic features of the dislocation content of solution grown crystals are now well-known and their origin generally understood. Of particular current interest is the way in which the dislocation structures of crystals of very large molecules such as proteins replicate those found in the very early work on ionic and small molecule crystals. It remains to be seen how the knowledge gained, from what may be regarded as relatively easy proteins to crystallize, can be translated into improved growth of more difficult systems.

Selecting and controlling growth conditions in respect of the location on the, often complex, phase diagram remains a key challenge in high temperature growth from fluxed melts, though when satisfactory crystals are grown, the dislocation density can be quite low. Such crystals often exhibit quite strong growth band contrast due to variations in composition during growth. Despite the importance of hydrothermal growth for production of quartz oscillators, the commercial drive to improve crystal quality seems to be in the area of production engineering, and relatively little academic work has appeared in recent years.

What is still not clear is the role of dislocations in determining crystal habit and growth rate dispersion. It has been observed that dislocations do enhance the growth speed of certain crystallographic faces, but whether screw or edge components dominate the change seems to be dependent on the material being grown. Nucleation of a screw dislocation may in itself change the growth mechanism from rough interface or birth and spread to spiral growth. It is also not clear exactly how the dislocation density influences any such growth rate enhancement or habit modification. The translation of the results of these detailed studies of very highly perfect crystals to an understanding of the industrial crystallization of microcrystals[70] remains a challenge.

AUTHOR INFORMATION

Corresponding Author

Brian K. Tanner − *Department of Physics, Durham University, Durham DH1 3LE, United Kingdom;* orcid.org/0000-0002-1474-177X; Email: b.k.tanner@dur.ac.uk

Complete contact information is available at: https://pubs.acs.org/10.1021/acs.cgd.2c01463

Notes

The author declares no competing financial interest.

DEDICATION

Dedicated to the memory of Prof. John Sherwood.

https://doi.org/10.1021/acs.cgd.2c01463
Cryst. Growth Des. 2023, 23, 3026−3033

REFERENCES

(1) Berg, W. Über eine röntgenographische Methode zur Untersuchung von Gitterstörungen und Kristallen. *Naturwissenschaften* **1931**, *19*, 391−396.
(2) Petit, A.; Pokam, S.; Mazen, F.; Tardiff, S.; Rieutord, F.; Landru, D.; Kononchuk, O.; Ben Mahomed, N.; Olbinado, M. P.; Rack, A. Brittle fracture studied by ultra-high-speed synchrotron X-ray diffraction imaging. *J. Appl. Crystallogr.* **2022**, *55*, 911−918.
(3) Barrett, C. S. A new microscopy and its potentialities. *Trans. Am. Inst. Mining Metall. Engineers* **1945**, *161*, 15−64.
(4) Schulz, L. G. Method of using a fine-focus X-ray tube for examining the surface of single crystals. *Trans. Am. Inst. Mining Metall. Engineers* **1954**, *200*, 1082−1083.
(5) Tuomi, T.; Naukkarinen, K.; Rabe, P. Use of synchrotron radiation in X-ray diffraction topography. *Phys. Stat. Sol. (a)* **1974**, *25*, 93−106.
(6) Bordas, J.; Glazer, M.; Hauser, H. The use of synchrotron radiation for X-ray topography of phase transitions. *Philos. Mag.* **1975**, *32*, 471−489.
(7) Tanner, B. K.; Safa, M.; Midgley, D.; Bordas, J. Observation of magnetic domain wall movements by X-ray topography using synchrotron radiation. *J. Magn. Mag. Mater.* **1976**, *1*, 337−341.
(8) Tanner, B. K. *X-ray Diffraction Topography*; Pergamon Press: Oxford, 1976.
(9) Bowen, D. K.; Tanner, B. K. *High resolution X-ray diffractometry and topography*; Taylor and Francis: London, 1998.
(10) Bowen, D. K.; Tanner, B. K. *X-ray Metrology in Semiconductor Manufacturing*; CRC Taylor and Francis: Boca Raton, 2006.
(11) Lider, V. V. X-ray Diffraction Topography Methods (Review). *Phys. Solid State* **2021**, *63*, 189−214.
(12) Danilewsky, A. N. X-Ray Topography - More than Nice Pictures. *Crystal Res. Technol.* **2020**, *55*, 2000012.
(13) Lang, A. R. Direct Observation of Individual Dislocations by X-Ray Diffraction. *J. Appl. Phys.* **1958**, *29*, 597−598.
(14) Hou, W. B.; Ristic, R. I.; Srinivasan, K.; Vrcelj, R. M.; Hammond, R. B.; Sheen, D. B.; Sherwood, J. N. Crystal Growth of the Acentric Organic Nonlinear Optical Material Methyl-p-hydroxybenzoate: Morphological Variations in Crystals Grown by Physical Vapor Transport. *Cryst. Growth Des.* **2019**, *19*, 5505−5515.
(15) Lang, A. R. The projection topograph: a new method in X-ray diffraction microradiography. *Acta Crystallogr.* **1959**, *12*, 249−250.
(16) Ikeno, S.; Maruyama, H.; Kato, N. X-ray topographic studies of NaCl crystals grown from aqueous solution with Mn ions. *J. Cryst. Growth* **1968**, *3-4*, 683−693.
(17) Emara, S. H.; Lawn, B. R.; Lang, A. R. Direct observation of dislocations in potash alum. *Philos. Mag.* **1969**, *19*, 7−12.
(18) Duckett, R. A.; Lang, A. R. The growth of nearly perfect hexamethylenetetramine crystals from solution. *J. Cryst. Growth* **1973**, *18*, 135−142.
(19) Authier, A. X-ray topography as a tool in crystal growth studies. *J. Cryst. Growth* **1972**, *13*, 34−38.
(20) Klapper, H. Defects in Non-Metal Crystals. In *Characterization of Crystal Growth Defects by X-ray Methods*, Tanner, B. K.; Bowen, D. K., Eds.; Plenum Press: New York, 1980; pp 133−160.
(21) Klapper, H.; Zaitseva, N.; Carman, L. X-ray topographic study of growth defects of trans-stilbene crystals grown from solutions. *J. Cryst. Growth* **2015**, *429*, 74−81.
(22) Klapper, H. X-ray Diffraction Topography: Application to Crystal Growth and Plastic Deformation. In *X-ray and Neutron Dynamical Diffraction, Theory and Applications*, Authier, A.; Lagomarsino, S.; Tanner, B. K., Eds.; Plenum Press: New York, 1996; pp 167−176.
(23) Hooper, R. M.; Roberts, K. J.; Sherwood, J. N. X-ray topographic investigations of dislocations in sodium chlorate. *J. Mater. Sci.* **1983**, *18*, 81−88.
(24) Klapper, H. Elastische Energie und Vorzugsrichtungen geradliniger Versetzungen in aus der Lösung gewachsenen organischen Kristallen. *Phys.Stat. Sol. (a)* **1972**, *14*, 99−106.
(25) Klapper, H. Elastische Energie und Vorzugsrichtungen geradliniger Versetzungen in aus der Lösung gewachsenen organischen Kristallen. II. Thioharnstoff. *Phys. Stat. Sol. (a)* **1972**, *14*, 443−451.
(26) Klapper, H. Preferred directions of dislocation lines in crystals grown from solution. *Acta Crystallogr., Sect. A* **1975**, *31*, S212.
(27) Klapper, H. Röntgen-topographischen Untersuchungen am lithiumformiat-monohydrat. *Z. Naturforsch.* **1973**, *28a*, 614−622.
(28) Klapper, H.; Küppers, H. Directions of dislocation lines in crystals of ammonium hydrogen oxalate hemihydrate grown from solution. *Acta Crystallog. A* **1973**, *29*, 495−503.
(29) Finnie, S. D.; Ristic, R. I.; Sherwood, J. N.; Zikic, A. M. Morphological and growth rate distributions of small self-nucleated paracetamol crystals grown from pure aqueous solutions. *J. Cryst. Growth* **1999**, *207*, 308−318.
(30) Smolsky, I. L.; Voloshin, A. E.; Zaitseva, N. P.; Rudneva, E. B.; Klapper, H. X-ray topographic study of striation formation in layer growth of crystals from solutions. *Philos. Trans. R. Soc. London A* **1999**, *357*, 2631−2649.
(31) Halfpenny, P. J.; Roberts, K. J.; Sherwood, J. N. Dislocations in energetic materials. 2. Characterization of the growth-induced dislocation structure of pentaerythritol tetranitrate (PETN). *J. Appl. Crystallogr.* **1984**, *17*, 320−327.
(32) Gallagher, H. G.; Vrcelj, R. M.; Sherwood, J. N. The crystal growth and perfection of 2,4,6-trinitrotoluene. *J. Cryst. Growth* **2003**, *250*, 486−498.
(33) Gallagher, H. G.; Sherwood, J. N.; Vrcelj, R. M. The growth and perfection of β-cyclotetramethylene-tetranitramine (HMX) studied by laboratory and synchrotron X-ray topography. *J. Cryst. Growth* **2017**, *475*, 192−201.
(34) Lang, A. R.; Muiscov, V. F. Dislocations and fault surfaces in synthetic quartz. *J. Appl. Phys.* **1967**, *38*, 2477−2483.
(35) Shinohara, A. H.; Iano, M. C.; Suzuki, C. K. New seed geometry for growth of low dislocation synthetic quartz. *I.E.E.E Trans. Ultrasonics, Ferroelectrics and Frequency Control* **2000**, *47*, 1199−1203.
(36) Homma, S.; Iwata, M. X-ray topography and EPMA studies of synthetic quartz. *J. Cryst. Growth* **1973**, *19*, 125−132.
(37) Epelboin, Y.; Zarka, A.; Klapper, H. Étude théorique et expérimentale d'énergie de dislocations. *J. Cryst. Growth* **1973**, *20*, 103−108.
(38) Lefaucheux, F.; Robert, M.; Authier, A. Étude des défauts créés lors de perturbations extérieures imposées au cours de la croissance hydrothermale de calcite. *J. Cryst. Growth* **1973**, *19*, 329−337.
(39) Tanner, B. K. Assessment of crystal perfection by X-ray topography. In *Surface and Defect Properties of Solids Vol. 6*, Roberts, M. W., Thomas, J. M., Eds.; The Chemical Society: London, 1977; pp 280−307.
(40) Takiyama, H.; Tezuka, N.; Matsuoka, M.; Ristic, R. I.; Sherwood, J. N. Growth rate enhancement by microcrystals and the quality of resulting potash alum crystals. *J. Cryst. Growth* **1998**, *192*, 439−447.
(41) Sherwood, J. N.; Shripathi, T. Role of dislocations in the growth of single crystals of potash alum. *Faraday Discuss.* **1993**, *95*, 173−182.
(42) Sherwood, J. N.; Shripathi, T. Evidence for the role of pure edge dislocations in crystal growth. *J. Cryst. Growth* **1988**, *88*, 358−364.
(43) Klapper, H.; Becker, R. A.; Schmiemann, D.; Faber, A. Growth-Sector Boundaries and Growth-Rate Dispersion in Potassium Alum Crystals. *Cryst. Res. Technol.* **2002**, *37*, 747−757.
(44) Masalov, V. M.; Zhokhov, A. A.; Manomenova, V. L.; Rudneva, E. B.; Voloshin, A. E.; Emelchenko, G. A. Growth of nickel sulfate hexahydrate (α-$NiSO_4.6H_2O$) single crystals under steady-state conditions of temperature difference. *Crystallogr. Rep.* **2015**, *60*, 963−969.
(45) Austerman, S. B.; Newkirk, J. B.; Smith, D. K. Study of Defect Structures in BeO Single Crystals by X-Ray Diffraction Topography. *J. Appl. Phys.* **1965**, *36*, 3815−3822.
(46) Tanner, B. K.; Smith, S. H. A study of the perfection of flux-grown rare earth vanadates by X-ray topography. *J. Cryst. Growth* **1975**, *28*, 77−84.

https://doi.org/10.1021/acs.cgd.2c01463
Cryst. Growth Des. 2023, 23, 3026−3033

(47) Safa, M.; Tanner, B. K.; Klapper, H.; Wanklyn, B. M. The direction of dislocations in flux-grown crystals. *Philos. Mag.* **1977**, *35*, 811−816.
(48) Jung, S.-T.; Kang, J.-K.; Chung, S.-J. Crystal growth and X-ray topography of $NdAl_3$ $(BO_3)_4$. *J. Cryst. Growth* **1995**, *149*, 207−214.
(49) Hu, X. B.; Wang, J. Y.; Cui, W. H.; Guan, Q. C.; Song, R. B.; Wei, J. Q.; Liu, Y. G.; Jiang, J. H.; Tian, Y. L. Growth defects in flux grown $RbTiOAsO_4$ crystals observed with white-beam synchrotron radiation topography. *J. Cryst. Growth* **1999**, *205*, 323−327.
(50) Gallagher, H. G.; Qi, X.; Sherwood, J. N.; Vrcelj, R. M. Crystal growth and characterisation of $KTiOAsO_4$. *J. Cryst. Growth* **2001**, *224*, 303−308.
(51) Izumi, K. Growth and lattice defects of hexamethylbenzene crystals. *J. Cryst. Growth* **1996**, *169*, 325−330.
(52) Lorber, B.; Sauter, C.; Ng, J. D.; Zhu, D. W.; Giegé, R.; Vidal, O.; Robert, M. C.; Capelle, B. Characterization of protein and virus crystals by quasi-planar wave X-ray topography: a comparison between crystals grown in solution and in agarose gel. *J. Cryst. Growth* **1999**, *204*, 357−368.
(53) Snell, E. H.; Cassetta, A.; Helliwell, J. R.; Boggon, T. J.; Chayen, N. E.; Weckert, E.; Holzer, K.; Schroer, K.; Gordon, E. J.; Zagalsky, P. F. Partial improvement of crystal quality for microgravity-grown apocrustacyanin C-1. *Acta Crystallogr.* **1997**, *D53*, 231−239.
(54) Volz, H. M.; Matyi, R. J. High-resolution X-ray diffraction analyses of protein crystals. *Philos. Trans. R. Soc. London* **1999**, *A357*, 2789−2799.
(55) Dobrianov, I.; Finkelstein, K. D.; Lemay, S. G.; Thorne, R. E. X-ray topographic studies of protein crystal perfection and growth. *Acta Crystallogr.* **1998**, *D54*, 922−937.
(56) Stojanoff, V.; Siddons, D. P.; Monaco, L. A.; Vekilov, P.; Rosenberger, F. X-ray topography of tetragonal lysozyme grown by the temperature-controlled technique. *Acta Crystallogr.* **1997**, *D53*, 588−595.
(57) Tanner, B. K. Dislocation contrast in X-ray topographs of very thin crystals. *Phys. Stat. Sol. (a)* **1972**, *10*, 381−6.
(58) Izumi, K.; Taguchi, K.; Kobayashi, Y.; Tachibana, M.; Kojima, K.; Ataka, M. Screw dislocation lines in lysozyme crystals observed by Laue topography using synchrotron radiation. *J. Cryst. Growth* **1999**, *206*, 155−158.
(59) Tachibana, M.; Koizumi, H.; Izumi, K.; Kajiwara, K.; Kojima, K. Identification of dislocations in large tetragonal hen egg-white lysozyme crystals by synchrotron white-beam topography. *J. Synchrotron Rad.* **2003**, *10*, 416−420.
(60) Koishi, M.; Ohya, N.; Mukobayashi, Y.; Koizumi, H.; Kojima, K.; Tachibana, M. Observation of clear images of dislocations in protein crystal by synchrotron monochromatic-beam X-ray topography. *Cryst. Growth and Design* **2007**, *7*, 2182−2186.
(61) Sawaura, T.; Fujii, D.; Shen, M.; Yamamoto, Y.; Wako, K.; Kojima, K.; Tachibana, M. Characterization of dislocations in monoclinic hen egg-white lysozyme crystals by synchrotron monochromatic-beam X-ray topography. *J. Cryst. Growth* **2011**, *318*, 1071−1074.
(62) Koizumi, H.; Uda, S.; Tsukamoto, K.; Kojima, K.; Tachibana, M.; Ujihara, T. Importance of hydration state around proteins required to grow high-quality protein crystals. *Cryst. Growth and Design* **2018**, *18*, 4749−4755.
(63) Koizumi, H.; Uda, S.; Tsukamoto, K.; Kojima, K.; Tachibana, M.; Ujihara, T. Importance of hydration state around proteins required to grow high-quality protein crystals. *Cryst. Growth and Design* **2018**, *18*, 4749−4755. Including Supporting Information.
(64) Suzuki, R.; Abe, M.; Kojima, K.; Tachibana, M. Identification of grown-in dislocations in protein crystals by digital X-ray topography. *J. Appl. Crystallogr.* **2021**, *54*, 163−168.
(65) Abe, M.; Suzuki, R.; Hirano, K.; Koizumi, H.; Kojima, K.; Tachibana, M. Existence of twisting in dislocation-free protein single crystals. *Proc. Nat. Acad. Sci.* **2022**, *119*, e2120846119.
(66) Koizumi, H.; Tachibana, M.; Yoshizaki, I.; Fukuyama, S.; Tsukamoto, K.; Suzuki, Y.; Uda, S.; Kojima, K. Dislocations in high-quality glucose isomerase crystals grown from seed crystals. *Cryst. Growth Des.* **2014**, *14*, 5111−5116.
(67) Abe, M.; Suzuki, R.; Kojima, K.; Tachibana, M. Evaluation of crystal quality of thin protein crystals based on the dynamical theory of X-ray diffraction. *IUCrJ.* **2020**, *7*, 761−766.
(68) Suzuki, R.; Koizumi, H.; Kojima, K.; Fukuyama, S.; Arai, Y.; Tsukamoto, K.; Suzuki, Y.; Tachibana, M. Characterization of grown-in dislocations in high-quality glucose isomerase crystals by synchrotron monochromatic-beam X-ray topography. *J. Cryst. Growth* **2017**, *468*, 299−304.
(69) Suzuki, R.; Baba, K.; Mizuno, N.; Hasegawa, K.; Koizumi, H.; Kojima, K.; Kumasaka, T.; Tachibana, M. Radiation-induced defects in protein crystals observed by X-ray topography. *Acta Crystall. D* **2022**, *78*, 196−203.
(70) Anuar, N.; Yusop, S. N.; Roberts, K. J. Crystallization of organic materials from the solution phase: a molecular, synthonic and crystallographic perspective. *Crystallog. Reviews* **2022**, *28*, 97−215.

https://doi.org/10.1021/acs.cgd.2c01463
Cryst. Growth Des. 2023, 23, 3026−3033